Journal of Basic and Environmental Sciences

ISSN
Online:2356-6388
Print:2536-9202

Research Paper Open Access

Kinetic studies on the catalyzed and un-catalyzed pyrolysis of mixed HDPE and PP (75:25 wt%) plastic waste using a combination of model-fitting and model-free methods

D.M. Fathy*, E.M. Kamar, M Hanafy, M.A. Mousa

Chemistry Department, Faculty of Science, Benha University, Benha, Egypt.

Corresponding author: E-mail address: doaamahmoud564@gmail.com

Abstract

This study investigates the catalyzed and un-catalyzed pyrolysis kinetics of waste samples composed of a commercial mixture of high-density polyethylene (HDPE) and polypropylene (75:25 wt%). The reaction mechanism and kinetic compensation effects were examined. Thermal analysis was conducted at various heating rates (β = 2–20°C/min) in an inert atmosphere using thermogravimetric analysis (TGA). Four methods—Friedman (FR), Ozawa-Flynn-Wall (OFW), Kissinger-Akahira-Sunose (KAS), and Starink (ST)—were employed to evaluate the kinetic parameters, including the pre-exponential factor and activation energy. Additionally, five model-fitting methods (Coats-Redfern, master plots, and iteration methods) were used to establish the kinetic model. The conversion function for random scission processes, f(R), is proposed to accommodate degradation mechanisms. The addition of a 10 wt% Zeolite A catalyst significantly reduced the activation energy required for the degradation of the waste mixture.

Keyword: Mixed Plastic, Kinetic model, Random Scission, Pyrolysis, catalysis.

1. Introduction

Due to their low price and adaptability, plastics significantly impact society. Around 400 million metric tons of plastic are produced annually, leading to significant garbage production and environmental issues [(1)]. Waste plastics are non-biodegradable and unsuitable for composting or landfilling [(2)]. Substitute recycling technologies are needed to address plastic waste disposal [(3, 4)]. Traditional landfilling uses land resources and waste

energy, while modern recycling techniques cause high labor costs and water pollution [5-7]. Advanced thermal treatments like pyrolysis are popular due to their volume reduction and energy recovery benefits [8, 9]. This straightforward, affordable, emission-reducing technique transforms waste plastic into valuable chemicals and hydrocarbon compounds [10, 11]. The effectiveness of catalysts depends on their chemical and physical properties. Catalysts enhance pyrolysis, influencing C-C bond breaking and chain length [12, 13]. Random scission is one of the most important mechanisms for the thermal cracking of poly olefins [14].

Understanding plastic waste pyrolysis is crucial for reactor design and optimization. Kinetic analysis is the primary method for pyrolysis, and thermos gravimetric analysis (TGA) measures mass loss. Continuous kinetics research over the entire temperature range is feasible, requiring less experimental data [15, 16]. Understanding thermal breakdown kinetics can improve plastics' thermal behavior [17, 18]. An excellent kinetic analysis requires determining the kinetic triplet, including the kinetic model, pre-exponential factor, A, and activation energy, E. This latter parameter is an algebraic expression linked to the physical model that characterizes the kinetics of a process. It is also referred to as the conversion function.

Polymer degradation kinetics is a complex process that is being debated. Model-free methods are common in the literature, but some assume first-order or "n-order" kinetic models without data [19, 20]. Recent studies show diffusion or random scission can control decomposition response. The thermal breakdown does not always follow first- or n-order kinetics.

The current study compares the quantitative characteristics of the 75% HDPE and 25% PP waste materials' catalyzed and un-catalyzed pyrolysis processes in a nitrogen environment. Several standard model-free techniques, including Freidman [21], Kissinger–Akahira–Sunose (KAS) [22], Flynn–Wall–Ozawa (FWO) [23], and Starink [24]methods, as well as Random session model and three model-fitting methods: Coats Redfern [25], iterative method [26], and Master Plots [27]. Determining the kinetic parameters helps to explain how much of a conversion occurs over time and how temperature affects reaction rate. The acquired kinetic parameters can be utilized for process parameter optimization, industrial plant design for pyrolysis, and scale-up methods. The calorimetric bomb was used to calculate the calorific value.

Zeolite A was employed in investigations of catalytic pyrolysis. Kinetic parameters help optimize processes, design industrial plants, and scale up methods in pyrolysis. Zeolite A was utilized as a catalyst in the study of catalytic pyrolysis. The calorimetric bomb was also used to calculate the calorific value.

2. Theory

Theoretical background

This section provided an overview of the fundamental theory of solid-state kinetic modeling used in this investigation [21-28]. Two main techniques are considered model-fitting methodology and model-free method. The model fitting provides insights into reaction processes and predicts kinetic parameters [29]. **Table s1** Appendix lists g(α) expressions for different reaction mechanisms employed in this study.

The TG results can be expressed in terms of mass change for solids or the degree of conversion (α):

$$\alpha = \frac{m_{0-}\ m_t}{m_{o-}m_f} \qquad (1)$$

Where m_0 and m_f refer to the initial and final sample weight, and m_t denotes the instant mass at time *t*.

The solid conversion rate ($\frac{d\alpha}{dt}$) can be stated as

$$\frac{d\alpha}{dt} = \beta\frac{d\alpha}{dT} = k(T)\ f(\alpha) \qquad (2)$$

Where β is the heating rate ($\frac{d\alpha}{dT}$, K/min), k(T) denotes the reaction rate constant depending on the temperature, and f(α) signifies the kinetic model function.

The k(T) can be defined according to the Arrhenius equation:

$$k(T) = Ae^{\frac{-E}{RT}} \qquad (3)$$

A represents the pre-exponential factor, E is the activation energy, and T and R symbolize the absolute temperature and universal gas constant, respectively. Combining equations (2) and (3) with a constant temperature ramp yields the following Equation:

$$\frac{d\alpha}{dT} = \frac{A}{\beta} - \ e^{\frac{-E}{RT}}\ f(\alpha) \qquad (4)$$

Kinetic Models

Coats Redfern (CR)

The CR method [25], developed by Coats and Redfern, is an integral model-fitting technique that estimates temperature integral using an asymptotic series expansion. By integrating Eq. 4, one may derive the integral version of the reaction model [29],

$$g(\alpha) = \int_0^a \frac{d\alpha}{f(a)} = \frac{A}{\beta}\int_0^T e^{-\frac{E}{RT}}\,dT = \frac{AE}{\beta R}\int_x^\alpha \frac{e^{-x}}{x^2}\,dx$$

$$= \frac{AE}{\beta R}p(x) \quad (5)$$

Where x equals ERT, the $p(x)$ is the temperature integral and has no analytical solution. There are many approximations of P(x) introduced in the literature [30], and one of them is given in Eq. 6

$$P(x) = (\exp\ \frac{x}{x^2}) \times (1+\frac{2!}{-x}) \quad (6)$$

Numerical integration or approximation is used to solve Eq. 5 and handle complex integrals, distinguishing model-free approaches. Introducing an approximation $p(x) = x^2e^{-x}$ $(20 \leqslant x \leqslant 50)$ into Eq. 5, the connection between inverse temperature and the heating rate becomes

$$g(\alpha) = \frac{ART^2}{\beta E}\left(1 - \frac{2RT}{E}\right) e^{\frac{-E}{RT}} \quad (7)$$

Taking the natural logarithm of both sides of Eq. 7 produces

$$\ln \frac{g(\alpha)}{T^2} = \ln \frac{AR}{\beta E}\left(1- \frac{2RT}{E}\right) - \frac{E}{RT} \quad (8)$$

Since 2RT/E << 1, the formula can be changed to

$$\ln \frac{g(\alpha)}{T^2} = \ln \left(\frac{AR}{\beta E}\right) - \frac{E_a}{RT} \quad (9)$$

When plotting $\ln \frac{g(\alpha)}{T^2}$ vs. $\frac{1}{T}$, a straight line is obtained for a fixed β and the postulated reaction mechanism g(α). One may ascertain E and A using the slope $\frac{-E}{R}$ and intercept ln $(\frac{AR}{\beta E})$.

KAS method

The KAS approach [22] was produced through the modification of Equation (8) to be

$$\text{Ln}\left(\frac{\beta_i}{T_{\alpha i}^2}\right) = \ln\frac{AR}{\frac{E\alpha}{g(\alpha)}} - \frac{E_\alpha}{RT_{\alpha i}} \quad (10)$$

The KAS method allows determining the apparent activation energy for a conversion value, α, by plotting ln $(\frac{\beta_i}{T_{\alpha i}^2})$ versus $\frac{1}{T_{\alpha i}}$ without a thorough understanding of the reaction process.

Friedman method (FR)

The Friedman method [21] is a popular differential iso conversional approach for determining activation energy as a function of α. It assumes that the mass loss rate is the only influencing factor, and by computing natural logarithms, it can be obtained. Consequently, it is possible to consider the f(α) as constant. By computing the natural logarithms of both sides of Eq. 4, one may obtain

$$\ln \beta\left(\frac{d\alpha}{dT}\right) = \ln [A\ f(\alpha)] - \frac{E_a}{RT} \quad (11)$$

Data abstraction for α and β values can be achieved through TG tests at different heating speeds, determining activation energy from the slope of the straight line obtained from the plot of ln $\beta(\frac{d\alpha}{dT})$ versus $\frac{1}{T}$.

FWO method

The FWO method is model-free [23] and uses Doyle's Equation to estimate the temperature integral [31]. After taking into account the approximation ln (x) = −5.331−1.052 x, Eq. (5) may be transformed into

$$\text{Ln } \beta = \ln\left(\frac{AE_a}{Rg(\alpha)}\right) - 5.331 - 1.052\,\frac{E_a}{RT} \qquad (12)$$

The activation energy can be determined by plotting ln β against 1/T, and the A values can be obtained from the intercept, ln $(\frac{AE_a}{Rg(\alpha)}$ −5.331).

Starink method (ST)

Integrating the approximation p(x)= e−1.0008x− $\frac{0.312}{x^{1.92}}$ into Eqs. (5) and (9), the relationship between heating rate and reversal temperature becomes

$$\ln\frac{\beta}{T^{1.92}} = -1.0008\,\frac{E_a}{RT} + C \qquad (13)$$

Many pairs of ln $\frac{\beta}{T^{1.92}}$ and $\frac{1}{T}$ may be derived at varying heating rates for a given series of α. When plotting ln $\frac{\beta}{T^{1.92}}$ versus $\frac{1}{T}$, a straight line should result; Eα may be calculated using the slope−1.0008 $\frac{E_a}{RT}$ [24].

Random scission kinetic model

The random scission kinetic model suggests that polymer chains undergo cleavage with first-order kinetics, resulting in decreasing lengths eventually released when evaporating [32]. However, establishing the link between volatilization mass and broken bond proportion is crucial [33]. The conversion function of this model was suggested to be

$$f(\alpha) = L\,(L-1)\,x\,(1-x)^{L-1} \qquad (14)$$

Where x and L stand for the minimal length of the nonvolatile polymer and the proportion of broken bonds, respectively, regretfully, Equation (13) only provides a symbolic solution for L = 2. The problem can be sorted out by calculating numerically the f(_α) functions for L ǂ2, just by giving values to both L and x.

Estimation Kinetic Models

The kinetic triplet, including activation energy, pre-exponential factor, and kinetic model, is crucial for accurate kinetic analysis of solid-state processes, especially in complex ones like polymer decomposition. Understanding the kinetic model helps manage processes, determine ideal processing temperatures, and conduct

aging studies. The most common procedure is fitting experimental data into predefined kinetic models or equations [34, 35]. Coats Redfern [25], Iterative method [26], and Master plots statistic [27] will be considered here as valuable methods for determining the kinetic mode in solid reactions.

The Iterative Procedure

In addition, the iterative procedure [26] is also applied to determine the solid kinetic model. The expression of the iterative procedure method, namely g(α) function is written as

$$\text{Ln}\,(g(\alpha))=(\ln A\, E_a\, R)+\ln(P(x)))-\ln\beta \quad (15)$$

Suppose the kinetic model can appropriately reflect the solid pyrolysis process. In that case, a linear relationship exists between ln(g(α)) versus lnβ, and the slope should be close to −1. The linear correlation coefficient R^2 is higher [36].

Master Plots

Ozawa's generalized kinetic Equation allows for creating universal master plots that can be used to analyze experimental data obtained with any heating profile [37]. Thus, if the definition of the generalized time is

$$\theta = \int_0^t \exp\frac{-E}{RT}dt \quad (16)$$

The θ denotes the duration required to get a specific α value at an infinite temperature. Equation (15), when differentiated, yields the following Equation:

$$\frac{d\theta}{dt} = \exp\left(\frac{E}{RT}\right) \quad (17)$$

Combining Equations (4 and 16) results in

$$\frac{d\alpha}{dt} = A\, f(\alpha) \quad (18)$$

which can also be expressed as:

$$\frac{d\alpha}{d\theta} = \frac{d\alpha}{dt}\exp\left(\frac{-E}{RT}\right) \quad (19)$$

Ozawa's equations (4, 18, and 19) provide the generalized reaction rate, dα/dθ, for extrapolating experimental data at infinite temperature, independent of the heating profile, and using α = 0.5 as a reference. Thus, Equation (19) yields the following, with α = 0.5 serving as a reference.

$$[(d\alpha/d\theta)/(d\alpha/d\theta)_{0.5}] = f(\alpha)/f(0.5)=\frac{P(x)}{P_{(x_{0.5})}} \quad (20)$$

To quantify the application of Equation (20), statistics number Z for estimating the fitness of each model is applied, as shown in Equations (21) and (22) [38].

$$S_j^2 = \frac{1}{n-1}\Sigma_{i=1}^{n}\left(\frac{P_i}{p_{0.5}} - \frac{g_i\,\alpha_i}{g_{jo.5}}\right)^2 \quad (21)$$

$$Z_j=\frac{s_j^2}{s_{min}^2} \quad (22)$$

Where i and j are the conversion rate and heating rate, respectively. If Z = 1 for each

heating rate of the model, it is considered a kinetic model of solid pyrolysis.

Generally, generalized master plots constructed from experimental data are faithful to the real system and allow discerning whether the reaction under study follows a theoretical model or deviates from such ideal situations.

3. Experimental

A commercial mixture of high-density polyethylene (HDPE) and PP waste samples (75: 25 wt %) used in this study were obtained from the market. Initially, the waste polymers were sun-dried for four days. Afterward, they were crushed in a mill to 3-5 mm particle size and placed within an airtight glass container to prevent moisture absorption. After that, they were cleansed with hot water and hexane to eliminate potential contamination. Hot air drying was then allowed for at least 24 hours at 60 degrees Celsius. The catalyst employed is Zeolite A, which was obtained from Alfa Aesar (Ward Hill, MA, USA). It has a specific area of 680 m^2/g and a pore volume of 0.127 nm.

TG analysis is the most widely used technique for studying the kinetics of thermal decomposition of solids. Thus, a thermos gravimetric Perkin Elmer TGA Diamond analyzer presented the kinetic analysis of the thermal decomposition of the catalyzed and un-catalyzed polymer samples. Around 10 mg of the sample was placed in a ceramic crucible on the sample holder of the balance and heated from 30°C to 700°C under a nitrogen gas flow of 3 L/min. The polymer sample was previously mixed with 10 wt% of the catalyst to obtain a homogeneous mixture. The experiments were performed at different heating rates of 2, 5, 10, and 20 K/min.

The Calorific value was determined using a Calorimetric Bomb IKA C-200 and about 0.5 g for 10 min with 99.5% pure oxygen. The calorific value obtained is 41.8 MJ/Kg.

4. Results and Discussion

The TG curves, Fig. 1 a, b show the pyrolysis of mixed plastic (HDPE+PP) and its catalyzed with Zeolite A at different heating rates of 2, 5, 10, and 20 ℃/min. The TG thermos grams show three decomposition steps for un-catalyzed sample and two for catalyzed sample, with weight loss curves displaced to higher temperatures with increasing heating rates. The 50% degradation for un-catalyzed mixed plastics occurred at 477 ℃, while catalyzed degradation occurred at 457 °C.

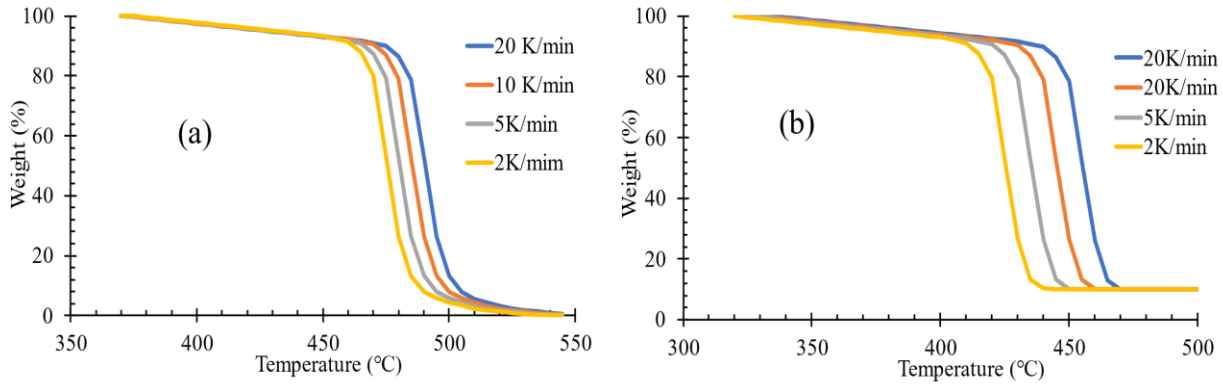

Fig. 1 Thermal decomposition at different heating rates for **a** mixed plastic of HDPE and PP (75: 25 wt%) and **b** catalyzed mixed plastic

Kinetic parameters of the pyrolysis process can be determined using various methods. However, comparing multiple methods with conversion values between 0.1 and 0.9 is recommended for accurate analysis due to instability at the beginning and ending periods and diffusion processes, as it generates temperature and partial pressure gradient [39, 40]. **Fig. 2** show typical plots for the KAS, FR, FWO, and ST model-free iso conversional methods constructed according to eq. (10, 11, 12 and 13) ,respectively, to evaluate the slopes of $\ln(\frac{\beta_i}{T_{\alpha i}^2})$ vs. $\frac{1}{T_{\alpha i}}$, $\ln \beta(\frac{d\alpha}{dT})$ vs. $\frac{1}{T}$, $\ln \beta$ vs. 1/, and $\ln \frac{\beta}{T^{1.92}}$vs. 1/T, respectively. **Fig. 3** show the same calculation methods for the catalyzed reactions. Linear regression analysis was used to obtain the values of activation energies in terms of α in the range of (0.1 - 0.9). The apparent activation energies (E_a) and square correlation factors were determined from the slope of regression lines provided in Table 1. The results show that the activation energies of the catalyzed process are less than those of the un-catalyzed reaction. The activation energy values achieved by KAS, FWO, and ST are almost close but higher than the FR method. The difference in calculated activation energy values can be attributed to improper integration errors in FWO, KAS, and ST equations. FR method uses instantaneous rate values and is very sensitive to the experimental noises. The dependence of apparent activation energy (E_a) on the degree of conversion (α) for the

decomposition process is presented in **Fig. 2,3**. A little dependence of E_a on α is observed in the conversion range of $0.20 \leq \alpha \leq 0.90$. However, the activation energy value is high at the start of the pyrolysis process, as it starts at strong polymer chain links and decreases as the reaction progresses. Since the average activation energy values worked out by the KAS, Straink, and FWO methods are very close, we choose the mean values of these three (at $0.20 \leq \alpha \leq 0.90$) as the value of activation energy used in the master plot method.

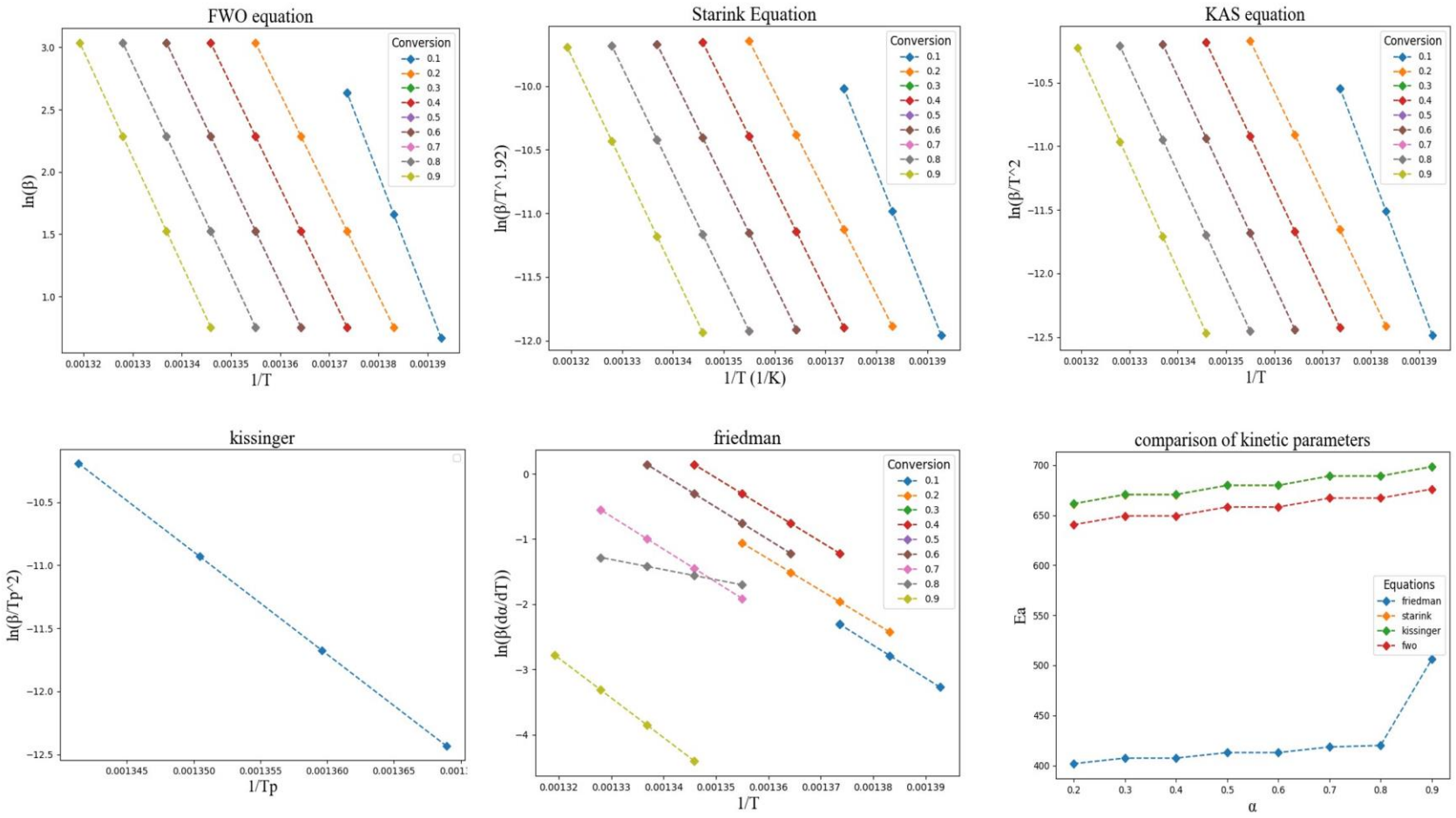

Fig. 2 The plots of the different kinetic models for the un-catalyzed pyrolysis of mixed plastic HDPE+PP (75:25 wt%) FWO, Starink, KAS, Kissinger, Friedman, conclusion curve.

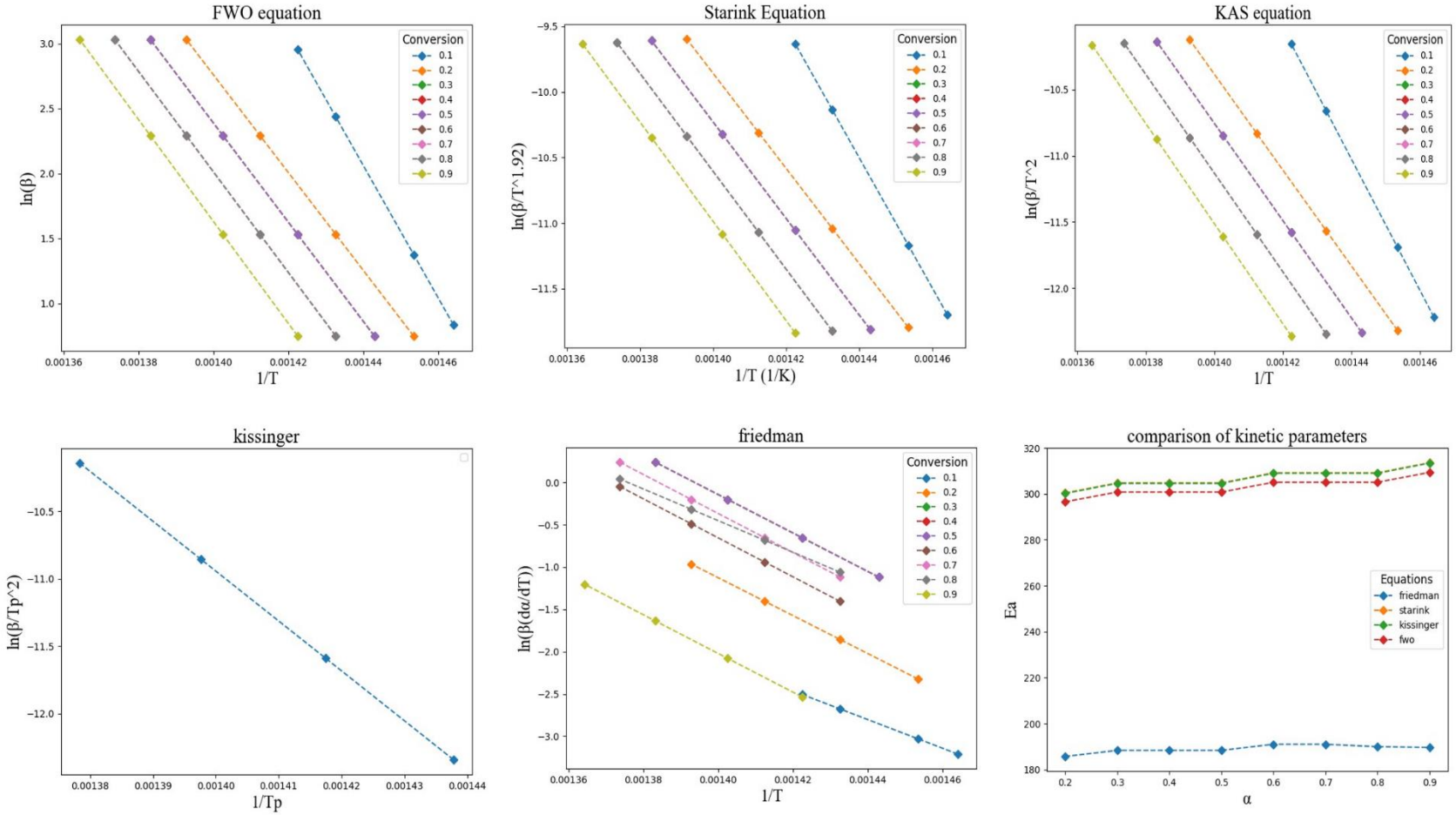

Fig. 3 The plots of the different kinetic models for the catalyzed pyrolysis of mixed plastic HDPE+PP (75:25 wt%) FWO ,Starink , KAS, Kissinger, Friedman, Conclusion curve.

Table 1 Kinetic data of different kinetic models for un-catalyzed and catalyzed pyrolysis of mixed plastics using 10 wt% of Zeolite A.

Conversion(α)	FWO		Starink		KAS		Freidman	
	E_a(kJ mol^{-1})	R^2	E_a (kJ mol^{-1})	R^2	E_a (kJ mol^{-1})	R^2	E_a (kJ mol^{-1})	R^2
0.1	767.71 (401.8)	0.916 (0.968)	795.48 (411.12)	0.914 (0.996)	795.65 (410.99)	0.914 (0.966)	395.87 (140.44)	0.968 (0.976)
0.2	605.86 (296.56)	0.996 (0.996)	625.296 (300.43)	0.995 (0.996)	625.32 (300.2)	0.995 (0.996)	380.1 (185.75)	0.979 (0.978)
0.3	614.41 (300.8)	0.996 (0.996)	634.21 (304.8)	0.995 (0.996)	634.24 (304.57)	0.995 (0.996)	385.47 (188.4)	0.988 (0.958)
0.4	614.41 (300.8)	0.996 (0.996)	634.21 (304.8)	0.995 (0.996)	634.24 (304.57)	0.995 (0.996)	385.47 (188.4)	0.988 (0.933)
0.5	623.03 (300.8)	0.996 (0.996)	643.18 (304.8)	0.995 (0.996)	643.22 (304.57)	0.995 (0.996)	390.88 (188.4)	0.978 (0.885)
0.6	623.03 (305.1)	0.996 (0.996)	643.18 (309.2)	0.995 (0.996)	643.22 (308.97)	0.995 (0.996)	390.88 (191.1)	0.957 (0.971)
0.7	631.71 (305.1)	0.996 (0.996)	652.22 (309.2)	0.995 (0.996)	652.26 308.97)	0.995 (0.996)	396.32 (191.1)	0.954 (0.968)
0.8	631.71 (305.1)	0.996 (0.996)	652.22 (309.2)	0.995 (0.996)	652.26 (308.97)	0.995 (0.996)	400.2 (190.22)	0.951 (0.996)
0.9	640.44 (309.4)	0.996 (0.996)	661.32 (313.63)	0.995 (0.996)	661.36 (313.4)	0.995 (0.996)	479.41 (189.69)	0.948 (0.964)
Average	639.1456 (313.9)		660.1462 (318.6)		660.197 (318.4)		400.55 (179.8)	

(catalyzed pyrolysis)

Estimation and Verification of Reaction Model

The CR method for TG data is used to determine the most probable mechanism function and calculate the pre-exponential factor. The method is based on getting a mechanism function with activation energy values at different heating rates, similar to free model methods [(41)]. The activation energy for all g(α) functions (listed in Appendix Table 1) was used to determine reliable reaction models. The resulting kinetic parameters are listed in Table 2. The most trustworthy reaction model is

identified by its higher R^2 value combined with a kinetic model's activation energy that is comparable to that found using a free kinetic approach. Under un-catalyzed pyrolysis, these requirements were found for the F_2 model and in catalyzed pyrolysis for the A_2 model. This indicates that the addition of a catalyst causes a decrease in the activation energy of the degradation process of the waste plastic with a change in the degradation model.

Table 2 Calculation results of E_a (kJ/mol) at different heating rates for un catalyzed and catalyzed HDPE +PP (75:25 wt%). based on the Coats Redfern model

Reaction Model	2 K/min		5 K/min		10 K/min		20 K/min		Average Value	
	E_a	R^2	E_a	R^2	E_a	R^2	E_a	R^2	E_a	R^2
$F_{1/3}$	351.17 (471.00)	0.8758 (0.9723)	351.71 (447.73)	0.8769 (0.9767)	352.31 (453.45)	0.8780 (0.9762)	366.78 (402.84)	0.9206 (0.9515)	355.49 (443.76)	0.88783 (0.9692)
$F_{3/4}$	426.32 (571.07)	0.9115 (0.9875)	427.87 (528.52)	0.9125 (0.9791)	429.47 (536.66)	0.9135 (0.9784)	436.79 (470.84)	0.9436 (0.9448)	430.11 (526.77)	0.92028 (0.9725)
$F_{3/2}$	608.57 (821.06)	0.9591 (0.9867)	612.76 (727.07)	0.9597 (0.9601)	617.01 (741.65)	0.9603 (0.9583)	605.24 (636.82)	0.9710 (0.9124)	610.9 (731.65)	0.96253 (0.9544)
F_2	761.86 (1034.22)	0.9758 (0.9704)	768.38 (894.86)	0.9761 (0.9354)	774.96 (915.07)	0.9764 (0.9331)	746.26 (776.52)	0.9773 (0.8818)	762.87 (905.17)	0.9764 (0.9302)
F_3	1122.37 (1533.08)	0.9860 (0.9341)	1134.43 (1286.2)	0.9859 (0.8875)	1146.54 (1319.6)	0.9858 (0.885)	1076.94 (1101.71)	0.9738 (0.8276)	1120.1 (1310.1)	0.98288 (0.8836)
$P_{3/2}$	460.54 (617.75)	0.8492 (0.9559)	460.499 (599.996)	0.8503 (0.9707)	460.55 (606.46)	0.8514 (0.9705)	488.49 (544.64)	0.9029 (0.9535)	467.52 (592.21)	0.86345 (0.9627)
$P_{1/2}$	145.35 (198.19)	0.8344 (0.9525)	145.28 (192.19)	0.8356 (0.9683)	145.24 (194.24)	0.8367 (0.9681)	154.53 (173.55)	0.8933 0.9494)	147.6 (189.54)	0.85 (0.9596)
$P_{1/3}$	92.82 (128.27)	0.8221 (0.9497)	92.74 (124.23)	0.8232 (0.9664)	92.69 (125.53)	0.8242 (0.9661)	98.87 (111.7)	0.8850 (0.9459)	94.28 (122.43)	0.83863 (0.957)
$P_{1/4}$	66.55 (93.3)	0.8084 (0.9467)	66.47 (90.24)	0.8094 (0.9642)	66.41 (91.18)	0.8104 (0.9639)	71.04 (80.77)	0.8759 (0.9421)	67.618 (88.87)	0.82603 (0.9542)
E_1	NAN (NAN)	NAN (NAN)	NAN (NAN)	NAN (NAN)	NAN (NAN)	NAN (NAN)	NAN (NAN)	NAN (NAN)	NAN (NAN)	NAN (NAN)
A_1, F_1	480.25 (644.2)	0.9303 (0.9915)	482.56 (586.94)	0.9312 (0.9763)	484.92 (596.93)	0.9321 (0.9752)	486.78 (519.8)	0.9552 (0.9369)	483.63 (586.97)	0.9372 (0.97)
$A_{3/2}$	316.09 (425.61)	0.9286 (0.9914)	317.59 (387.39)	0.9295 (0.9758)	319.14 (393.998)	0.9304 (0.9747)	320.37 (342.53)	0.9540 (0.9335)	318.3 (387.38)	0.93563 (0.9694)
A_2	234.00 (316.31)	0.9268 (0.9912)	235.11 (287.62)	0.9278 (0.9753)	236.25 (292.53)	0.9287 (0.9742)	237.16 (253.9)	0.9529 (0.9341)	235.63 (287.59)	0.93405 (0.9687)
A_3	151.92 (207.01)	0.9230 (0.9901)	152.63 (187.84)	0.9241 (0.9744)	153.36 (191.06)	0.9250 (0.9732)	153.96 (165.27)	0.9504 (0.9312)	152.97 (187.8)	0.93063 (0.9672)
A4	110.88	0.9190	111.39	0.9201	111.92	0.9211	112.35	0.9477	111.64	0.92698

	(152.36)	(0.9905)	(137.95)	(0.9733)	(140.33)	(0.9721)	(120.95)	(0.9280)	(137.9)	(0.966)
A_U	NAN	NAN	NAN	NAN	NAN	NAN	NAN	NAN	NAN	NAN
	(NAN)	(NAN)	(NAN)	(NAN)	(NAN)	(NAN)	(NAN)	(NAN)	(NAN)	(NAN)
R_1, F_0, P_1	302.94	0.8457	302.89	0.8468	302.89	0.8479	321.51	0.9007	307.56	0.86028
	(407.97)	(0.9551)	(396.09)	(0.9701)	(400.35)	(0.9699)	(359.09)	(0.9525)	(390.88)	(0.9619)
$R_2, F_{1/2}$	379.11	0.8905	380.02	0.8916	380.99	0.8927	392.87	0.9302	383.25	0.90125
	(507.94)	(0.9795)	(477.69)	(0.9786)	(484.29)	(0.9781)	(428.11)	(0.9497)	(474.51)	(0.9715)
$R_3, F_{2/3}$	409.86	0.9047	411.17	0.9058	412.55	0.9068	421.49	0.9394	413.77	0.91418
	(548.95)	(0.9853)	(510.75)	(0.9793)	(518.35)	(0.9786)	(455.92)	(0.9468)	(508.49)	(0.9725)
D_1	618.13	0.8509	618.12	0.8520	618.21	0.8531	655.47	0.9041	627.48	0.86503
	(827.53)	(0.9563)	(803.9)	(0.9709)	(812.57)	(0.9708)	(730.19)	(0.9539)	(793.55)	(0.963)
D_2	706.91	0.8759	707.95	0.8770	709.11	0.8781	739.08	0.9206	715.76	0.8879
	(943.04)	(0.9707)	(899.07)	(0.9763)	(910.39)	(0.9759)	(811.03)	(0.9528)	(890.88)	(0.9689)
D_3	831.96	0.9072	834.68	0.9083	837.52	0.9093	855.43	0.9410	839.9	0.91645
	(1109.49)	(0.9856)	(1033.22)	(0.9798)	(1048.58)	(0.9791)	(923.84)	(0.9481)	(1028.8)	(0.9732)
D_4	747.50	0.8874	749.08	0.8885	750.78	0.8895	776.88	0.9282	756.06	0.8984
	(669.73)	(0.9768)	(942.45)	(0.9783)	(955.05)	(0.9778)	(847.54)	(0.9518)	(853.69)	(0.9712)
D_5	1137.91	0.9519	1145.01	0.9527	1152.23	0.9533	1138.59	0.9676	1143.4	0.95638
	(1526.98)	(0.9902)	(1365.72)	(0.9674)	(1391.73)	(0.9659)	(1202.12)	(0.9230)	(1371.6)	(0.9616)
D_6	551.81	0.8404	551.25	0.8416	550.82	0.8428	590.15	0.8973	561.01	0.85553
	(740.35)	(0.9506)	(727.4)	(0.9693)	(734.35)	(0.9692)	(663.28)	(0.9557)	(716.35)	(0.9612)
D_7	572.98	0.8439	572.59	0.8451	572.33	0.8463	611.04	0.8996	582.24	0.85873
	(768.2)	(0.9526)	(751.9)	(0.9699)	(759.39)	(0.9698)	(684.73)	(0.9552)	(741.06)	(0.9619)
D_8	490.99	0.8286	489.97	0.8299	489.08	0.8313	530.03	0.8895	500.02	0.84483
	(660.28)	(0.9438)	(656.78)	(0.9668)	(662.16)	(0.9668)	(601.38)	(0.9569)	(645.15)	(0.9586)
G_1	204.54	0.7631	203.45	0.7639	202.42	0.7648	227.44	0.8447	209.46	0.78413
	(280.58)	(0.9001)	(288.68)	(0.9434)	(290.16)	(0.9436)	(266.87)	(0.9458)	(281.57)	(0.9332)
G_2	147.32	0.6993	145.79	0.6998	144.33	0.7002	170.78	0.8005	152.06	0.72495
	(205.12)	(0.8536)	(222.05)	(0.9178)	(222.04)	(0.9181)	(208.42)	(0.9359)	(214.41)	(0.9064)
G_3	110.57	0.6487	108.86	0.6486	107.22	0.6484	133.11	0.7644	114.94	0.67753
	(155.44)	(0.8148)	(176.31)	(0.8947)	(175.41)	(0.8951)	(167.57)	(0.9257)	(168.68)	(0.8826)
G_4	972.76	0.9319	977.44	0.9329	982.26	0.9337	986.01	0.9563	979.62	0.9387
	(1299.99)	(0.9917)	(1185.59)	(0.9767)	(1205.74)	(0.9756)	(1051.6)	(0.9382)	(1185.7)	(0.9706)
G_5	1465.26	0.9325	1472.33	0.9334	1479.59	0.9343	1485.23	0.9566	1475.6	0.9392
	(1955.77)	(0.9917)	(1784.25)	(0.9769)	(1814.55)	(0.9758)	(1583.4)	(0.9386)	(1784.5)	(0.9708)
G_6	1957.76	0.9327	1967.22	0.9337	1976.93	0.9345	1984.46	0.9568	1971.6	0.93943
	(2611.56)	(0.9917)	(2382.9)	(0.9769)	(2423.36)	(0.9758)	(2115.2)	(0.9388)	(2383.3)	(0.9708)
G_7	183.43	0.8838	183.84	0.8849	184.29	0.8861	190.21	0.9259	185.44	0.89518
	(248.18)	(0.9785)	(232.99)	(0.9776)	(236.21)	(0.977)	(208.06)	(0.9470)	(231.36)	(0.97)
G_8	198.80	0.8992	199.42	0.9003	200.07	0.9014	204.52	0.9358	200.7	0.90918
	(268.68)	(0.9846)	(249.52)	(0.9784)	(253.24)	(0.9776)	(221.96)	(0.9441)	(248.35)	(0.9712)

(Catalyzed pyrolysis)

The iteration and master plots methods were also used to determine possible kinetic

models for the degradation of mixed plastic. According to the iteration method, the slope of the plots of ln(g(α)) versus lnβ should be close to −1, and the linear correlation The master plots statistical method shows that if the Z-value of Eq.22 is equal to one for each heating rate of the investigated model, then the model is regarded as a kinetic model of solid pyrolysis. The results are given in **Table 3**. From which, the kinetic of the pyrolysis is better describe by the random scission model [32, 33]. This model assumes that the cleavage of bonds occurs randomly along the polymeric chains, followed by the volatilization of the fragments once they are small enough. The coefficient R^2 is high [36]. The results are listed in **Table 3**. From which, the kinetic of the pyrolysis can be better described by the random scission model.

differences between the F_1 and random scission models can be attributed to the initial mass loss during chain cleavage. As the reaction progresses, the polymer chains shorten, producing small fragments that evaporate. This leads to the system cooling down to maintain the reaction rate. However, both conversion functions become similar, indicating that a first-order model with high values cannot describe a random scission-driven process.

Table 3 Reaction mechanisms data determined by master plots and the iterative procedure methods for un-catalyzed reaction and catalyzed reaction

No.	g(α)	Master plot method				ln(g(α)) vs. lnβ	
		2K/min	5 K/min	10K/min	20 K/min	Slope	R 2
P2	$\alpha^{1/2}$	3.96 (4.91)	5.14 (6.34)	1.51 (2.54)	4.11 (5.61)	0.639 (0.721)	0.9424 (0.9355)
P_3	$\alpha^{1/3}$	1.54 (2.13)	2.78 (3.88)	1.24 (2.32)	2.29 (3.55)	0.717 (0.828)	0.9552 (0.9351)
P_4	$\alpha^{1/4}$	11.64 (9.51)	0.19 (2.32)	0.61 (0.99)	0.04 (0.24)	0.877 (0.866)	0.9652 (0.9412)
$P_{3/2}$	$\alpha^{3/2}$	3.17 (6.18)	3.00 (4.01)	1.30 (2.36)	2.58 (3.38)	0.959 (0.949)	0.9654 (0.9534)
$P_{2/3}$	$\alpha^{2/3}$	9.08	4.03	1.37	2.67	0.959	0.9212

		(11.2)	(5.03)	(2.26)	(3.18)	(0.933)	(0.9116)
$P_{3/4}$	$\alpha^{3/4}$	11.41 (13.55)	8.31 (9.66)	5.22 (6.24)	3.45 (4.36)	0.8832 (0.8643)	0.8734 (0.9121)
F_1	$-\ln(1-\alpha)$	4.18 (5.13)	1.47 (1.88)	1.05 (4.05)	1.24 (1.33)	0.767 (0.774)	0.8864 (0.8942)
F_2	$(1-\alpha)^{-1}-1$	102.66 (99.55)	4.37 (5.12)	0.18 (0.23)	2.61 (4.44)	0.999 (0.889)	0.9823 (0.9934)
F_3	$(1/2)[(1-\alpha)^{-2}\ 1]$	1335.39 (99.66)	87.80 (86.83)	0.98 (0.65)	61.10 (77.34)	1.277 (3.65)	0.9818 (0.9833)
A_1	$\alpha^{3/2}$	11.61 (22.55)	2.78 (12.66)	1.26 (7.88)	2.38 (4.55)	0.876 (0.886)	0.9882 (0.9812)
$A_{1.5}$	$[-\ln(1-\alpha)]^{2/3}$	3.40 (7.40)	12.5 (11.5)	94 1.57 (54.5)	4.63 (8.13)	0.511 (0.612)	0.9911 (0.9821)
A_2	$[-\ln(1-\alpha)]^{1/2}$	69.58 (59.51)	8.91 (8.71)	1.82 (6.22)	6.82 (7.62)	0.384 (0.364)	0.9929 (0.9829)
A_3	$[-\ln(1-\alpha)]^{1/3}$	40.34 (44.14	21.23 (11.13)	12.73 (10.53)	11.65 (11.85)	0.776 (0.716)	0.8891 (0.8791)
A_4	$[-\ln(1-\alpha)]^{1/4}$	26.11 (28.31)	15.18 (16.28)	11.42 (10.32)	9.53 (9.83)	0.694 (0.774)	0.8342 (0.7642)
R_1	α	48.30 (54.25)	6.93 (16.83)	1.69 (11.61)	5.47 (5.37)	0.669 (0.659)	0.9881 (0.9781)
R_2	$1-(1-\alpha)^{1/2}$	23.50 (13.58)	4.19 (4.17)	41 3. (41 3.)	39.7 (29.5)	0.584 (0.664)	0.9942 (0.9912)
R_3	$1-(1-\alpha)^{1/3}$	15.82 (24.82)	3.24 (8.14)	1.30 (2.45)	2.65 (3.35)	0.995 (0.921)	0.9945 (0.9835)
D_1	α^2	0.63 (0.77)	0.299 (0.389)	0.83 (0.87)	0.40 (0.51)	1.167 (1.27)	0.988 (0.9781)
D_2	$\alpha+(1-\alpha)\ln(1-\alpha)$	21.53 (19.53)	0.31 (0.51)	0.50 (0.45)	0.17 (0.37)	1.274 (1.15)	0.992 (0.9921)

D_3	$[1-(1-\alpha)^{1/3}]^2$	121.99 (88.77)	5.37 (45.27)	0.14 (0.34)	3.41 (3.51)	1.401 (1.39)	0.995 (0.9942)
D_4	$1-2\alpha/3-(1-\alpha)^{2/3}$	43.19 (40.19)	1.17 (1.18)	0.37 (0.39)	0.67 (0.77)	1.316 (1.21)	0.993 (0.9951)
R.S.	L=8	0.9961 (0.9916)	0.9955 (0.9955)	0.9944 (0.9944)	0.9977 (0.9977)	1.094 (1.094)	0.9981 (0.9981)

(catalyzed pyrolysis)

5. Conclusion

The study conducted TG experiments under non isothermal conditions at four different constant heating rates of 2, 5, 10, and 20 °C/min to examine the pyrolysis kinetics for a catalyzed and un-catalyzed commercial mixture of high-density polyethylene (HDPE) and PP waste samples (75% HDPE and 25% PP). Results showed that the pyrolysis process of the un-catalyzed process occurred in three stages, with weight losses of 2.80-3.02%, 94.45-95.11%, and 0.04-0.16%, respectively. At the same time, the pyrolysis of the catalyzed mixed plastic occurs at lower temperatures in two steps. The increase in heating rate shifted the pyrolysis process to a higher temperature zone. Based on the TG analysis, the activation energy and linear correlation coefficient were determined at different conversion rates using four model-free methods (FWO, KAS, Starink, and Friedman method) and three kinetic methods (including CR, Master plot, and iterative procedure) were applied to estimate the conversion rate with the comparison of experimental data. The activation energy values achieved by KAS, FWO, and ST are almost close but higher than the FR method. An average activation energy obtained from KAS identical, FWO, and ST methods was used to determine the kinetic model. The Random Scission model gave higher R^2 values out of the CR methods, and the calculated E_a values were comparable to the average values from the three methods. The activation energy of the catalyzed pyrolysis was less than the un-catalyzed pyrolysis. The close similarity between the experimental conversion function and that corresponding to random scission proved that the latter is the mechanism driving the decomposition of mixed plastic.

Ethical Approval:

Institutional Review Board Statement: The research was carried out and authorized in compliance with the ethical committee's declaration (code:BUFS-REC-2024-234 Chm) of Benha University's Faculty of Science.

6. References

1. Geyer, R.; Jambeck, J. R.; Law, K. L. (2017). Production, use, and fate of all plastics made. *Sci. Adv.*, 3, e1700782.

2. Ozaki, J. I.; Djaja, S. K. I.; Oya, A. (2000). Preparation of Activated Carbons from Kelp and Their Application to the Electrochemical Double Layer Capacitor. *Ind. Eng. Chem. Res.*, 39, 245.

3. Stelmachowski, M. (2010). Thermal conversion of waste polyolefins to the mixture by hydrocarbons in the reactor with molten metal bed. *Energy Convers. Manag.*, 51(10), 2016-2020. http://dx.doi.org/10.1016/j.enconman.2010.02.035

4. Abbas-Abadi, M. S.; Haghighi, M. N.; Yeganeh, H. (2012). The effect of temperature, catalyst, different carrier gases and stirrer on the produced transportation hydrocarbons of LLDPE degradation in a stirred reactor. *J. Anal. Appl. Pyrolysis*, 95, 198-204. http://dx.doi.org/10.1016/j.jaap.2012.02.007

5. Li, Y.; Li, J.; Deng, C. (2014). Occurrence, characteristics and leakage of polybrominated diphenyl ethers in leachate from municipal solid waste landfills in China. *Environ. Pollut.*, 184, 94–100.

6. Datta, J.; Kopczyńska, P. (2016). From polymer waste to potential main industrial products: Actual state of recycling and recovering. *Crit. Rev. Environ. Sci. Technol.*, 46, 905–946.

7. Deng, C.; Li, Y.; Li, J.; et al. (2017). Emission characteristics of PBDEs during flame-retardant plastics extruding process: Field investigation and laboratorial simulation. *Environ. Sci. Pollut. Res.*, 24, 22450–22457.

8. Cheng, S.; Qiao, Y.; Huang, J.; et al. (2019). Effects of Ca and Na acetates on nitrogen transformation during sewage sludge pyrolysis. *Proc. Combust. Inst.*, 37, 2715–2722.

9. Yu, S.; Su, W.; Wu, D.; et al. (2019). Thermal treatment of flame retardant plastics: A case study on a waste TV plastic shell sample. *Sci. Total Environ.*, 675, 651–657.

10. Qi, W.; Liu, G.; He, C.; et al. (2019). An efficient magnetic carbon-based solid acid treatment for corncob saccharification with high selectivity for xylose and enhanced enzymatic digestibility. *Green Chem.*, 21, 1292–1304.

11. Sharuddin, S. D. A.; Abnisa, F.; Daud, W. M. A. W.; et al. (2016). A review on pyrolysis of plastic wastes. *Energy Convers. Manag.*, 115, 308–326.

12. López, A.; De Marco, I.; Caballero, B. M.; Adrados, A.; Laresgoiti, M. F. (2011). Deactivation and regeneration of ZSM-5 zeolite in catalytic pyrolysis of plastic wastes. *Waste Manag.*, 31(8), 1852-1858. http://dx.doi.org/10.1016/j.wasman.2011.04.004

13. Serrano, D. P.; Aguado, J.; Escola, J. M.; Rodríguez, J. M. (2005). Influence of nanocrystalline HZSM-5 external surface on the catalytic cracking of polyolefins. *J. Anal. Appl. Pyrolysis*, 74(1-2), 353-360. http://dx.doi.org/10.1016/j.jaap.2004.11.037

14. Das, S. (2007). Pyrolysis and catalytic cracking of municipal plastic waste for recovery of gasoline range hydrocarbons. *A Thesis, National Institute of Technology*, Rourkela.

15. Mishra, G.; Kumar, J.; Bhaskar, T. (2015). Kinetic studies on the pyrolysis of pinewood. *Bioresour. Technol.*, 182, 282-288.

16. Jeur, R. V.; Gerun, L.; Tazerout, M.; Catelain, C.; Bellettre, J. (2008). Dimensional modelling of wood pyrolysis using a nodal approach. *Fuel*, 87, 3292-3303.

17. Vyazovkin, S.; Wight, C. A. (1998). Isothermal and nonisothermal kinetics of thermally stimulated reactions of solids. *Int. Rev. Phys. Chem.*, 17, 407-433.

18. Friedman, H. L. (1964). Kinetics of thermal degradation of char-forming plastic from thermogravimetry: Application to a phenolic plastic. *J. Polym. Sci. Part C*, 6, 183-195.

19. Habibi, A.; De Wilde, J. (2007). Kinetic modeling of the thermal degradation of methacrylate copolymers by thermogravimetric methods. *Int. J. Chem. React. Eng.*, 5, 18.

20. Mamleev, V.; Bourbigot, S.; Le Bras, M.; Yvon, J.; Lefebvre, J. (2006). Model-free method for evaluation of activation energies in modulated thermogravimetry and analysis of cellulose decomposition. *Chem. Eng. Sci.*, 61, 1276.

21. Friedman, H. (1963). Kinetics of chain depolymerization. *J. Polym. Sci. C*, 6, 183.

22. Akahira, T.; Sunose, T. (1971). Method of determining activation deterioration constant of electrical insulating materials. *Res. Rep. Chiba Inst. Technol.*, 16, 22-31.

23. Flynn, J. H.; Wall, L. A. (1966). General treatment of the thermogravimetric of polymers. *J. Res. Natl. Bur. Stand. A*, 70, 487-523.

24. Starink, M. J. (1996). A new method for the derivation of activation energies from experiments performed at constant heating rate. *Thermochim. Acta*, 288, 97-104.

25. Coats, A. W.; Redfern, J. P. (1964). Kinetic parameters from thermogravimetric data. *Nature*, 201, 68.

26. Li, L.; Chen, D. (2004). Application of iso-temperature method of multiple rate to kinetic analysis. *J. Therm. Anal. Calorim.*, 78, 283–293.

27. Sánchez-Jiménez, P. E.; Pérez-Maqueda, L. A.; Perejón, A.; Criado, J. M. (2010). Generalized kinetic master plots for the thermal degradation of polymers following a random scission mechanism. *J. Phys. Chem. A*, 114, 7868–7876. https://doi.org/10.1021/jp103171h

28. Buda, V.; et al. (2020). Solid State Stability and Kinetics of Degradation for Candesartan—Pure Compound and Pharmaceutical Formulation. *Pharmaceu.*, 12, 86. https://doi.org/10.3390/pharmaceutics12020086.

29. Çepelioğullar, Ö.; Haykırı-Açma, H.; Yaman, S. (2016). Kinetic modelling of RDF pyrolysis: Model-fitting and model-free approaches. *Waste Manag.*, 48, 275–284.

30. Farjas, J.; Roura, P. (2011). Isoconversional analysis of solid state transformations. *J. Therm. Anal. Calorim.*, 105, 757–766.

31. Doyle, C. D. (1965). Series approximations to the Equation of thermogravimetric data. *Nature*, 207, 290-291. doi:10.1038/207290a0.

32. Simha, R.; Wall, L. A. (1952). Kinetics of chain depolymerization. *J. Phys. Chem.*, 56, 707–715.

33. Sanchez-Jimenez, P. E.; Perez-Maqueda, L. A.; Perejon, A.; Criado, J. M. (2010). A new model for the kinetic analysis of thermal degradation of polymers driven by random scission. *Polym. Degrad. Stab.*, 95, 733–739.

34. Gotor, F. J.; Criado, J. M.; Malek, J.; Koga, N. (2000). Kinetic analysis of solid-state reactions:

the universality of master plots for analyzing isothermal and nonisothermal experiments. *J. Phys. Chem. A*, 104, 10777–10782.

35. Sanchez-Jimenez, P. E.; Perez-Maqueda, L. A.; Perejon, A.; Criado, J. M. (2010). Generalized kinetic master plots for the thermal degradation of polymers following a random scission mechanism. *J. Phys. Chem. A*, 114, 7868–7876.

36. Shahcheraghi, S.; Khayati, G.; Ranjbar, M. (2015). An advanced reaction model determination methodology in solid-state kinetics based on Arrhenius parameters variation. *J. Therm. Anal. Calorim.*, 122, 175–188.

37. Criado, J.; Ortega, A.; Gotor, F. (1990). Correlation between the shape of controlled-rate thermal analysis curves and the kinetics of solid-state reactions. *Thermochim. Acta*, 157, 171–179.

38. Jiang, L.; Zhang, D.; Li, M.; He, J.; Gao, Z.; Zhou, Y.; Sun, J. (2018). Pyrolytic behavior of waste extruded polystyrene and rigid polyurethane by multi kinetics methods and Py-GC/MS. *Fuel*, 222, 11–20.

39. Koga, N.; Criado, J. M. (1998). Kinetic analyses of solid-state reactions with a particle-size distribution. *J. Am. Ceram. Soc.*, 81, 2901–2909.

40. Ding, Y.; Ezekoye, O. A.; Lu, S.; et al. (2017). Comparative pyrolysis behaviors and reaction mechanisms of hardwood and softwood. *Energy Convers. Manag.*, 132, 102–109.

41. Koga, N.; Criado, J. M. (1998). The influence of mass transfer phenomena on the kinetic analysis for the thermal decomposition of calcium carbonate by constant rate thermal analysis (CRTA) under vacuum. *Int. J. Chem. Kinet.*, 30, 737–744.